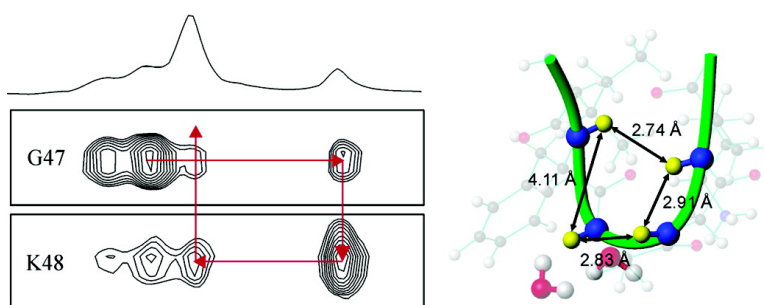## Communication

# High-Sensitivity Observation of Dipolar Exchange and NOEs between Exchangeable Protons in Proteins by 3D Solid-State NMR Spectroscopy

Eric K. Paulson, Corey R. Morcombe, Vadim Gaponenko,
Barbara Dancheck, R. Andrew Byrd, and Kurt W. Zilm

## More About This Article

Additional resources and features associated with this article are available within the HTML version:

- Supporting Information
- Links to the 12 articles that cite this article, as of the time of this article download
- Access to high resolution figures
- Links to articles and content related to this article
- Copyright permission to reproduce figures and/or text from this article

View the Full Text HTML

# High-Sensitivity Observation of Dipolar Exchange and NOEs between Exchangeable Protons in Proteins by 3D Solid-State NMR Spectroscopy

Eric K. Paulson,[†] Corey R. Morcombe,[†] Vadim Gaponenko,[‡] Barbara Dancheck,[‡] R. Andrew Byrd,[‡] and Kurt W. Zilm*,[†]

*Department of Chemistry, Yale University, P.O. Box 208107, New Haven, Connecticut 06520-8107, and Structural Biophysics Laboratory, National Cancer Institute, Frederick, Maryland 21702*

Received July 26, 2003; E-mail: kurt.zilm@yale.edu

While NMR structures of proteins are nearly always for molecules in solution, the vast majority of protein structures have been obtained by X-ray diffraction on frozen crystals. Problems posed by membrane proteins, insoluble protein aggregates, and differences between some X-ray and solution NMR structures all provide compelling reasons for developing robust solid-state NMR (ssNMR) methods for determination of protein structure. A great deal of progress has been made in this regard in the past decade. Approaches for obtaining full $^{13}$C and $^{15}$N assignments[1-4] and for assigning backbone amide $^1$H shifts[5] have been demonstrated on small proteins or peptides. A wide range of techniques have been developed to measure $^{13}$C−$^{13}$C, $^{13}$C−$^{15}$N, and $^{15}$N−$^{15}$N distances.[6-8] Such methods, in combination with patterned isotopic enrichment, produced the first ssNMR structure of a small crystalline protein domain in the past year.[9]

These pioneering advances, relying on heteronuclei, have been impressive technical accomplishments. However, if ssNMR is to approach solution methods in scope and capability, techniques that exploit the higher sensitivity and larger distance measuring range of $^1$H's must be developed. The experimental realization of $^1$H detection for high-resolution magic angle spinning (MAS) $^1$H/$^{15}$N heteronuclear single quantum coherence (HSQC) ssNMR spectroscopy makes deployment of 3D methods and the measurement of tertiary contacts between $^1$Hs very much more feasible.[10-12] In this Communication, we report a new 3D ssNMR technique analogous to the $^1$H-detected 3D $^1$H/$^{15}$N HSQC NOESY method. We demonstrate that this sensitive 3D spectroscopy can confirm assignments of backbone amide resonances and observe long-range contacts in application to a $\beta$-turn in human ubiquitin.

Figure 1 diagrams the basic pulse sequence developed. This is intended for application to exchangeable $^1$H's in $^{15}$N- and $^2$H-enriched protein samples, where the combination of magnetic dilution and fast MAS has been shown by us[12] to provide average $^1$H line widths of only 0.22 ppm. $^1$H evolution in $t_1$ under WALTZ-16 $^{15}$N decoupling and MAS at $\sim$20 kHz is projected onto the spin-lock field in the first cross-polarization (CP) step. Magnetization is transferred to $^{15}$N, which evolves for $t_2$ under $^1$H decoupling, and the desired frequency-labeled component is projected onto the z-axis by a $\pi/2$ pulse. While this $^{15}$N magnetization is stored along z, the $^1$H decoupling is continued so that the experiment operates in a constant power mode regardless of the length of $t_2$. This is key to reducing $t_2$ noise as well as being a central ingredient in efficient water suppression. A further delay of $t_w$ of $\sim$10 ms provides for dephasing of unwanted transverse magnetization. $^1$H magnetization that is frequency labeled by $^1$H chemical shift in $t_1$ and $^{15}$N chemical shift in $t_2$ is then created with a second CP step and immediately placed along the z-axis. Spin exchange of several
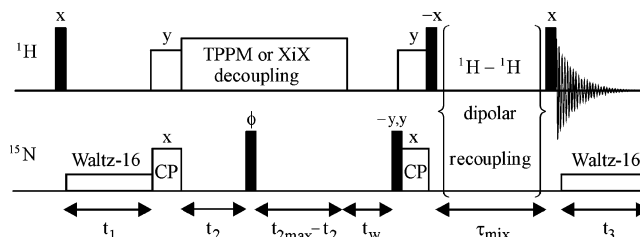
---

**Figure 1.** Pulse sequence for 3D ssHSQC-detected dipolar exchange spectroscopy. Solid bars represent $\pi/2$ pulses. The $^1$H $\pi/2$ pulse length is 2.4 $\mu$s, and the $^{15}$N $\pi/2$ pulse length is 4.6 $\mu$s. TPPM decoupling was performed at 100 kHz. CP transfers use a $^{15}$N rf field of $\sim$55 kHz and a $^1$H rf field of $\sim$75 kHz with a spin rate of $\sim$20 kHz. $t_{2max} = 30$ ms, and $t_{1max} = 5$ ms. The phase $\phi$ is switched between $-y$ and $x$ phases to acquire quadrature data in $t_2$. The $^{15}$N RF level is set to $\sim$2.5 kHz during WALTZ-16 decoupling. The $^1$H carrier frequency is placed on the water resonance. The $^{15}$N $\pi/2$ pulse, prior to final CP and receiver phase, is switched between $y$ and $-y$ on alternate scans. For a description of the 800-MHz instrument used and other experimental conditions, see ref 12.

types can then occur during the period $\tau_{mix}$. We have used RFDR[13] as a $^1$H−$^1$H dipolar recoupling method in this work, but any number of other longitudinal or transverse techniques can be applied.[6,14] After the appropriate mixing time, the magnetization is placed in the xy plane, and a high-resolution $^1$H MAS spectrum acquired.

For magnetization originating on the kth amide $^1$H, the real component of the 3D time domain signal is of the form

$$S_k(t_1,t_2,t_3) = \sum_m a_k \cos(\omega_{H_k}t_1)\cos(\omega_{N_k}t_2)\cos(\omega_{H_k}t_3) +$$
$$c_{km}\cos(\omega_{H_k}t_1)\cos(\omega_{N_m}t_2)\cos(\omega_{H_m}t_3)$$

where the sum extends over the m amides that exchange or cross-relax with k during $\tau_{mix}$. Each $\omega_1$ plane has an autopeak of intensity $a_k$ and cross-peaks for each of the m exchange partners with amplitudes $c_{km}$. Autopeaks fall on the line $\omega_1 = \omega_3$ in any $\omega_1$ plane. Walks through the protein start by picking an autopeak, moving along $\omega_2$ to find cross-peaks at frequencies $\omega_3'$, and continuing by confirmation of an autopeak in the corresponding plane at $\omega_1' = \omega_3'$. An example is provided in Figure 2, showing strip plots for the $\beta$-turn in ubiquitin comprising residues F45−K48. This particular data set used RFDR for 1.2 ms as the dipolar recoupling during $\tau_{mix}$. Other experimental details are listed in the figure caption, but it should be noted that this very high signal-to-noise result was acquired on just 500 nmol of protein in only 48 h. We estimate the 200 largest of the over 300 peaks picked by computer search would easily be identified with half the signal-to-noise, or acquired in one-fourth the time. The autopeaks for A46 and G47 in ubiquitin are outliers and are assigned on the basis of similarity to the solution NMR shifts.[15]

K48 and F45 can be assigned on the basis of this walk. Other short segments in the protein can be also be walked just as readily.
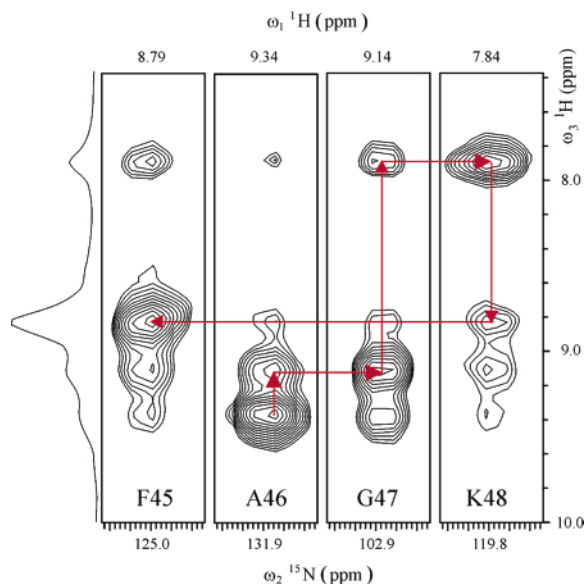
**Figure 2.** Strip plots of $\omega_2\omega_3$ planes at $\omega_1$ shift indicated at top. Each strip is 1 ppm wide in $\omega_2$ and centered at the $^{15}$N shift indicated. Signal-to-noise ratio is indicated by the slice taken through the leftmost strip. Forty-eight $t_1$ points were acquired using a dwell time of 104 $\mu$s in $t_1$, and 96 complex points were acquired in $t_2$ using a dwell time of 312 $\mu$s. $^1$H carrier was placed on the water resonance. Sixteen scans per point, 1 s recycle delay, $^1$H resonance frequency 799.55 MHz. The walk from A46 back to F45 shown in red. The ubiquitin sample was prepared using 2-methyl-2,4-pentanediol-$d_{12}$ as precipitant, as described in ref 12.
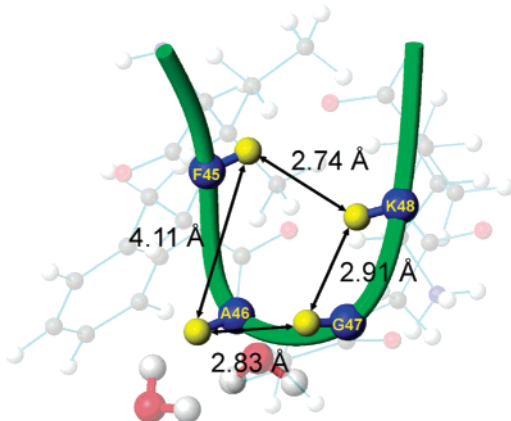


**Figure 3.** Depiction of the $\beta$-turn comprised of F45−K48 in ubiquitin, showing the interspin distances involved. The water molecules closest to A46 and G47 are also shown.

Cross-peaks corresponding to all possible $^1$H−$^1$H contacts among these four spins are observed. To the left of Figure 2 is a slice taken along the $\omega_3$ axis for F45, indicating the relative intensities of the autopeaks and cross-peaks. The strongest cross-peak for F45 is across the turn to K48, while the weakest is the sequential cross-peak with A46. This is the expected result if the $\beta$-turn structure in this crystal form[16] is similar to that in the reported X-ray structure.[17] Adding hydrogens to the crystal structure,[18] the $^1$H contacts involved in this turn are calculated to cover the range of 2.7−4.3 Å. Some of these are indicated in the structural diagram in Figure 3. As the cross-peak intensities would indicate, the K48 and F45 amide protons are quite close, being separated by only 2.74 Å, while the corresponding A46−F45 distance is much longer, at 4.11 Å. Full utilization of the many contacts observed of this type will require a complete independent assignment of the $^{15}$N and $^1$H shifts, and this work is in progress.

In addition to amide-to-amide cross-peaks, many amides have cross-peaks with bound water. The kinetics of the magnetization exchange of individual amides with water can readily be studied by setting $t_1$ to zero in the pulse sequence of Figure 1, and collecting 2D spectra as a function of $\tau_{mix}$. An even simpler measurement is to also set $t_2$ to zero and follow the $\tau_{mix}$ time course of the amide and crystal water bands in 1D spectra. In this manner, an average cross-relaxation time constant of $\sim$90 s$^{-1}$ is observed, independent of whether dipolar recoupling is used. However, if the exchange is monitored in the rotating frame by extending the final $y$-phase $^1$H CP pulse into $\tau_{mix}$ and eliminating the pair of flip up and down $^1$H pulses, the kinetics are quite different. These observations are consistent with the amide-to-water magnetization exchange being NOE relaxation in the solid state, as opposed to chemical exchange[19] or spin flips due to static dipolar interactions.

In summary, a sensitive solid-state analogue of the 3D $^1$H/$^{15}$N HSQC-detected NOESY experiment has been described, and long-range nonsequential $^1$H−$^1$H contacts have been observed. The method provides an entry to structure determination in nanocrystalline $^{15}$N/$^2$H-enriched protein samples and is expected to have its greatest utility in study of the physical chemistry and dynamics of proteins. In this vein, the observation of numerous NOEs between amide protons and structural water highlights the type of information we expect this new approach will provide in the study of macromolecular systems.

**References**

(1) McDermott, A.; Polenova, T.; Bockmann, A.; Zilm, K. W.; Paulson, E. K.; Martin, R. W.; Montelione, G. T. *J. Biomol. NMR* **2000**, *16*, 209−219.
(2) Straus, S. K.; Bremi, T.; Ernst, R. R. *J. Biomol. NMR* **1998**, *12*, 39−50.
(3) Rienstra, C. M.; Hohwy, M.; Hong, M.; Griffin, R. G. *J. Am. Chem. Soc.* **2000**, *122*, 10979−10990.
(4) Pauli, J.; Baldus, M.; van Rossum, B.; de Groot, H.; Oschkinat, H. *ChemBioChem* **2001**, *2*, 272−281.
(5) van Rossum, B. J.; Castellani, F.; Pauli, J.; Rehbein, K.; Hollander, J.; de Groot, H. J. M.; Oschkinat, H. *J. Biomol. NMR* **2003**, *25*, 217−223.
(6) Baldus, M. *Prog. Nucl. Magn. Reson. Spectrosc.* **2002**, *41*, 1−47.
(7) Hohwy, M.; Rienstra, C. M.; Griffin, R. G. *J. Chem. Phys.* **2002**, *117*, 4973−4987.
(8) Jaroniec, C. P.; Filip, C.; Griffin, R. G. *J. Am. Chem. Soc.* **2002**, *124*, 10728−10742.
(9) Castellani, F.; van Rossum, B.; Diehl, A.; Schubert, M.; Rehbein, K.; Oschkinat, H. *Nature* **2002**, *420*, 98−102.
(10) Reif, B.; Griffin, R. G. *J. Magn. Reson.* **2003**, *160*, 78−83.
(11) Chevelkov, V.; van Rossum, B. J.; Castellani, F.; Rehbein, K.; Diehl, A.; Hohwy, M.; Steuernagel, S.; Engelke, F.; Oschkinat, H.; Reif, B. *J. Am. Chem. Soc.* **2003**, *125*, 7788−7789.
(12) Paulson, E. K.; Morcombe, C. R.; Gaponenko, V.; Dancheck, B.; Byrd, R. A.; Zilm, K. W. *J. Am. Chem. Soc.* **2003**, *125*, in press.
(13) Bennett, A. E.; Ok, J. H.; Griffin, R. G.; Vega, S. *J. Chem. Phys.* **1992**, *96*, 8624−8627.
(14) Karlsson, T.; Popham, J. M.; Long, J. R.; Oyler, N.; Drobny, G. P. *J. Am. Chem. Soc.* **2003**, *125*, 7394−7407.
(15) Wang, A. C.; Grzesiek, S.; Tschudin, R.; Lodi, P. J.; Bax, A. *J. Biomol. NMR* **1995**, *5*, 376−382.
(16) Igumenova, T. I. *Assignment of uniformly carbon-13-enriched proteins and optimization of their carbon line shapes*; Columbia University: New York, 2003; p 199.
(17) Vijaykumar, S.; Bugg, C. E.; Cook, W. J. *J. Mol. Biol.* **1987**, *194*, 531−544.
(18) Word, J. M.; Lovell, S. C.; Richardson, J. S.; Richardson, D. C. *J. Mol. Biol.* **1999**, *285*, 1735−1747.
(19) Grzesiek, S.; Bax, A. *J. Biomol. NMR* **1993**, *3*, 627−638.

JA037559U